Progress towards a widely-usable integrated silicon photonic photon-pair source

CHAOXUAN MA,[1] XIAOXI WANG,[1] AND SHAYAN MOOKHERJEA[1,*]

[1] *University of California, San Diego, Department of Electrical and Computer Engineering, La Jolla, California 92093-0407, USA*
[*] *smookherjea@ucsd.edu*

Abstract: Photon-pair generation at telecommunication wavelengths using high-quality silicon microring resonators is an active area of research. Here, we report on significant progress towards the ultimate goal of an integrated silicon microchip for bright generation of photon pairs with multiple stages of tunable optical filtering on the same chip. A high pair generation brightness of 6.5×10^{10} pairs/s/mW^2/nm is achieved. The resonance of the high-Q silicon microring resonator can be monitored using a high dynamic range readout of a photocurrent in an all-silicon p-i-n diode fabricated across the waveguide cross-section, which is used to align the ring resonance to the passbands or stopbands of the filters.

1. Introduction

Over the last decade, an integrated photonic approach is becoming increasingly attractive for quantum information processing (QIP) applications [1-5]. Some integrated photonic microchips which generate and use single photons or entangled photons have been demonstrated on silicon-on-insulator (SOI) platform [4,5] for certain demanding QIP applications. However, progress towards inexpensive and robust integration of quantum optical sources in manufacturable platforms (e.g., wafer-scale foundry-fabricated silicon photonics) for widespread applications, such as quantum key distribution in large scale networks, is still incomplete. There is a growing need for such devices, in order to scale up the development of quantum communication links in multi-user networks. The rapidly-growing library of integrated device components in silicon photonics can be fabricated in large volumes using cost-effective wafer-scale processing, and thus possesses the potential to address the needs for a low-cost, yet high-performance and high-brightness photon-pair source microchip at telecommunications wavelengths.

Different approaches to on-chip integration of photon sources offer possible solutions at various wavelength ranges. Among the most popular devices are quantum dots [6], devices that generate photons from color centers [7] and nonlinear photonic devices [8-13]. Of these, the latter are most suitable at the wavelengths near 1550 nm which are compatible with low-loss fiber optics transmission. With a strong third-order nonlinearity, entangled photon pairs can be generated in silicon waveguides and micro-resonators via spontaneous four wave mixing (SFWM). For example, a high quality of photon pair generation in the laboratory has been demonstrated in several high-Q (quality factor) silicon photonic microring resonator devices, as reviewed in Ref. [13]. Under SFWM, energy-conservation between the pump (P) and the generated signal (S) and idler (I) photons dictates the frequency relationship $2\omega_P = 2\omega_S+\omega_I$ and all three frequencies lie within the band used in wavelength-division multiplexed (WDM) communication networks near 1550 nm.

Quantum optical communication receivers will incorporate filters before the single photon detectors; however, some degree of optical filtering is also needed at the source, so that additional noise processes that may degrade the photon quality are mitigated. Source devices based on high-Q microrings as part of a multi-component microchip also need a convenient method of monitoring of the resonance. Here, progress is demonstrated towards the engineering

development of a single-chip, inexpensive and low-cost solution for bright generation of photon pairs for quantum communication. In this work, we address the integration design and challenges of the tunable passive components, including the microring used for pair generation and the microring-based tunable filters. We do not address here the laser itself, which in separate research has been studied either through hybrid integration of a dedicated laser [14] or coupling of laser light from external platforms [15-18].

2. Device design and experimental details

The microchip was fabricated by a foundry silicon photonic process on SOI wafers, which has a silicon layer of 230 nm on top of 2 μm thick buried oxide. There are three filtering stages of this chip and a summary of the component specifications is listed in **Table 1,** comparing the design intention with the experimentally-measured result on the fabricated chip. Figure 1(a) shows a photograph of the fabricated chip. The photonic chip was wire-bonded with a PCB board and attached to the center of a brass board together with a thermistor and a heat sink to keep the chip temperature controlled using an external TEC controller. The chip was designed to guide the lowest-order TE-polarized waveguide mode. Other polarizations should be stripped out by various features on the chip, including bends and rib-to-ridge waveguide transitions. Light was coupled into and out of the chip by on-chip inverse tapers and edge-coupled polarization-maintaining fiber arrays, as shown in Fig. 1(a). The insertion loss of each fiber-to-waveguide coupler was estimated as ~7 dB averaged over the wavelengths of interest, based on separate measurements at test sites which include straight waveguides with similar taper structures at the edges.

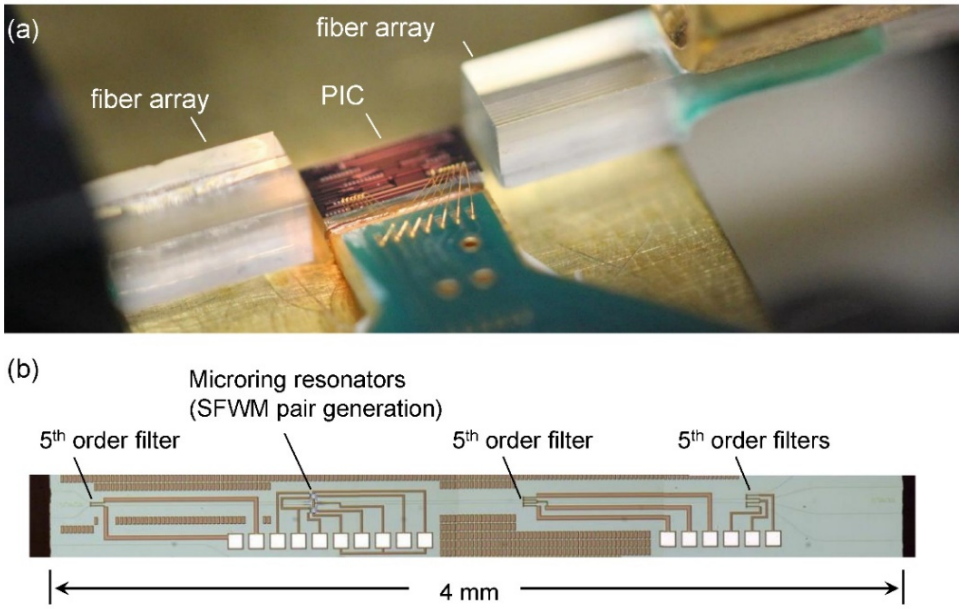

Fig. 1 (a) Photograph of the wire-bonded chip and the fiber arrays used for edge coupling to tapered waveguides. (b) Composite optical microscope image of the chip, showing the various stages. The electrical wirebonds and wiring traces are also visible. (PIC: Photonic Integrated Circuit. CROW: Coupled Resonator Optical Waveguide optical filter configuration). The photonic chip consists of a micro-resonator for photon pair generation and a few stages of tunable optical filters.

Figure 1(b) shows the layout of the chip, which has a first filtering stage, the microring resonator used for pair generation, and two additional stages of filters. The light path from the input to the output of the chip traverses sixteen microring resonators, which serve various functions. SFWM in microrings relies on the generation of correlated photons at the signal and

idler frequencies, spaced symmetrically around the pump frequency by one or more multiples of the resonator free spectral range (FSR) [19,20]. This makes it convenient to use microring filters, rather than other types of filters (e.g., Bragg filters), for the filter stages, since the free spectral range (FSR) of the filter microrings can be harmonically related to the FSR of the SFWM microring, as described below.

Microring resonator for pair generation using SFWM

A critical component on the pair generation chip is the high-Q microring used for optically-pumped SFWM. The microring which was designed as an all-pass resonator, using partially-etched ridge silicon waveguides of width 600 nm and slab thickness 70 nm and slab width of about 1.9 μm. To comprise this ring resonator, four Bezier quarter-bends were used, as shown in Fig. 2(a), each designed with a radius of R = 10 μm. Bezier bends achieve lower bending loss than a simple quarter-circle, leading to a higher Q factor and thus, a higher pair generation rate. The width of the coupling gap is about 0.34 μm.

An in-built mechanism is provided to monitor the resonance of the high-Q resonator without requiring an external photodiode. Using p and n implants, followed by via formation and metalization (as part of the foundry process) a p-i-n diode was built in the cross-section of the partially-etched silicon waveguide used for the microring resonator. P-type dopants consist of Boron at an areal density of about 5 x 10^{15} cm^{-2}, and n-type dopants consist of Phosphorous at a density of about 3.5 x 10^{15} cm^{-2}.The dopants were placed far from the middle of the waveguide, in order to minimize the optical loss. When the optical circulating power is high (i.e., the microring is driven by a pump laser whose wavelength is on resonance), there is a weak, but easily measured photocurrent (see measurements below) which is proportional to the optical power circulating in the microring [21]. The electrical readout of this diode (under a typical bias of -1 V) provides a simple and convenient indicator whether the microring resonance wavelength is aligned to the wavelength of the pump laser, and is particularly helpful when tuning the device or the laser to compensate for thermo-optic resonance shifts. The achieved dynamic range here is an improvement on what we previously reported in Ref. [21].

Table 1 Summary of Component Specifications

Chip section	Free Spectral Range		Full-width at half maximum	
	designed	measured	designed	measured
First-stage filter	10 nm	11 nm	1 nm	4 nm
Microring resonator (pair generation)	5 nm	4.93 nm	0.006 nm	0.011 nm
Second-stage filter	10 nm	11 nm	1 nm	4 nm
Third-stage filter	7.5 nm	9.3 nm	1 nm	4.7 nm

Coupled microring resonator filters

The first filter serves to carve notches in the incoming spectrum, at the wavelengths at which the entangled photon pairs will be generated. Note that this filter may not be needed if low-noise laboratory grade lasers (such as Ref. [22]) are used. However, this filter was included since it was noted in Ref. [14] that if a bare-die laser is used as the pump, the level of the amplified spontaneous emission (ASE) noise floor can be quite high. The design of this filter requires a specific relationship between the FSR of the pair-generation microring and that of the filter. The simplest such relationship is FSR(ring) = FSR(filter)/2, which results in pairs of symmetrically-spaced spectral notches being carved at the signal and idler frequencies (or equivalently, wavelengths), and the pump frequency being allowed through with low insertion

loss. Because of the harmonic relationship, it is helpful to fabricate the filter on the same chip as the microring resonator.

The filter which follows the microring diverts the residual pump light to a different pathway, so that the rate of further SFWM or noise from spontaneous Raman scattering in the main photonic circuit is lowered. The third-stage optical filter was intended to serve to demultiplex the signal and idler photons. However, fabrication errors resulted in this filter also serving mainly to suppress the pump a bit further. Note that this chip is not intended to achieve the highest possible on-chip filtering (e.g., Refs. [23,24]) which may be required when integrating detectors on the same chip. In a typical quantum communication or QKD system over a network [25,26], it is reasonable to assume that the detectors are some distance away from the sources, and incorporate their own filters. Our primary goal here is to prevent additional SFWM or scattering processes in long waveguides on the source chip itself from corrupting the quantum state after it is prepared by the microring. Since the rate of additive noise photons scales with the residual pump power, any extra attenuation of the residual pump light is helpful. With about 45 dB of net pump rejection achieved here, the rate of such processes, proportional to the square of the pump power, would be suppressed by nine orders of magnitude.

The optical filters each consist of five coupled-microring resonators in the CROW (coupled resonator optical waveguide [27]) configuration using fully-etched strip waveguides. For these microrings as well, four Bezier quarter-bends were used in each "ring", rather than simple quarter bends. However, since the Q factor is lower, and therefore, the thermo-optic resonance shift was less of a concern, compared to the pair generation microring, the monitoring diode is not needed. Therefore, the microrings which make up the filters were designed using fully-etched waveguides, without the slab region and the dopants, which allow for a tight bending effective radius of 5 μm.

All filters and the microring used for SFWM have metal heaters above to shift their filter passbands or ring resonances, which are formed with minimum geometry serpentines. The heaters were fabricated using a Ti/TiN/AlCu/TiN metal stack that is less than 1 μm thick. The heater efficiencies were measured to be about 0.05 nm/mW for the filters and about 0.08 nm/mW for the ring.

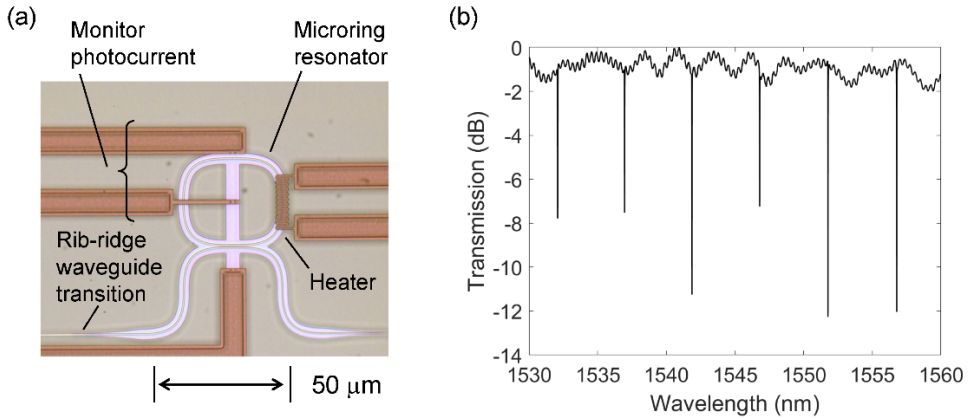

Fig. 2(a) Microscope image of the microring resonator used for pair generation, also showing the electrical contact lines and the serpentine metal heater used for thermally tuning the resonance. (b) Measured transmission resonances from a test chip in which the microring segment was diced out from the other sections.

3. Results

The fabricated microring resonator which is used for photon-pair generation was tested. From a separate chip, in which the microring portion was diced out for testing, the transmission spectrum was measured with a swept-wavelength laser between 1530 nm and 1560 nm

wavelengths and is shown in Fig. 2(b). From this measurement, the free-spectral range (FSR) of the microring was determined to be 4.93 nm ± 40 pm in the vicinity of 1550 nm.

On the combined chip, the actual microring used for the pair generation experiment was measured to have a loaded quality factor of 1.4×10^5 at 1550 nm, with a spectral full-width at half-maximum (FWHM) of 1.4 GHz, as shown in Fig. 3 (black line). The spectrum was measured by first locating the resonance using a swept-wavelength scan at low power, and then activating the tuners (thermal heaters) of the first-stage filter and the third-stage filters to align their passbands with the microring resonance. Searching for the resonance of the high-Q ring was assisted by measuring and monitoring the photocurrent from the reverse-biased p-i-n diode, as shown in Fig. 3 (red line). The measurement of an improved value of the microring quality factor (Q) suggests that the optical propagation loss in the waveguide was adequately low (less than 2 dB/cm at 1550 nm) compared to previous-reported results [13].

The next set of reported results is about the monitoring of the microring resonance using the reverse bias diode fabricated across the ridge waveguide. The current, which is proportional to the circulating optical intensity of the pump field, is induced by a photo-transition of an electron from the valence band to a mid-bandgap state, and transitioning to the conduction band assisted by the electric field. Here, a reverse bias of -1 V resulted in a generated current of about 160 nA at resonance. For off-resonance, the current was significantly less, and we achieved an on-off contrast of more than 30 dB (without requiring a change of the amplifier gain or bias). Such a current is easily measurable by low-noise integrated or off chip electronics and is adequate for monitoring the resonance of the microring. The slight mismatch between the spectral dip and photocurrent peak could be due to imperfect scan synchronization between the instruments or a result of uncontrolled ambient temperature variation in the measurement setup. The value of this monitoring photodiode in a multi-stage photonic circuit, with several tunable stages, is significant, since the transmission spectrum of the ring alone cannot always be measured. Moreover, this electronic readout provides a more useful, sensitive and convenient monitoring mechanism for the high-Q microring resonance than, for example, looking at the microring with an infrared camera [28].

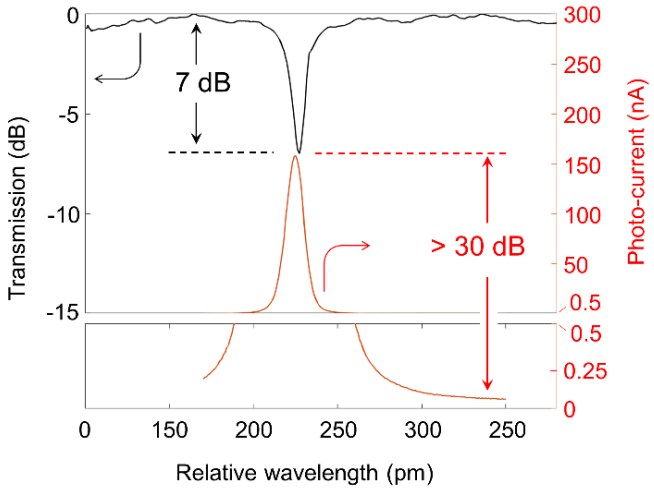

Fig. 3 The black line (left-hand side vertical axis) shows the ring resonance (transmitted optical power in dB versus wavelength shift in picometers, relative to 1553.100 nm) measured using a swept-wavelength tunable laser. The red line (right-hand side vertical axis) shows the resonance-monitoring photo-current, which was also measured when sweeping the laser wavelength. The lower panel uses a different vertical scale and shows more clearly the (low) noise floor of the photo-current.

The complete chip, despite some fabrication imperfections in the current batch which are discussed below, was able to generate photon pairs when optically pumped with continuous-

wave (CW) light. The pump wavelength was generated using a laboratory-grade diode laser [22] and was positioned at 1553.2 nm and signal and idler photons were detected at 1543.3 nm and 1563.3 nm, respectively. Photons were detected using fiber-coupled superconducting (WSi) nanowire single photon detectors (SNSPD), cooled to 0.8 K in a closed-cycle Helium-4 cryostat equipped with a sorption stage. The detection efficiencies for the SNSPDs were about 68% as measured using separate calibration measurements. These detectors were not gated and were operated in a simple dc-biased mode with an RF-amplified readout. Coincidences were measured using a multi-input time-to-digital converter (TDC) instrument, with 10 ps bin width, in start-stop mode. To filter the background, external tunable filters (benchtop components) were used at these three wavelengths with FWHM's of approximately 1 nm, 0.6 nm and 0.8 nm, respectively, which are much wider than the spectral width of the photons, estimated by the linewidth of the ring resonance to be about 0.011 nm.

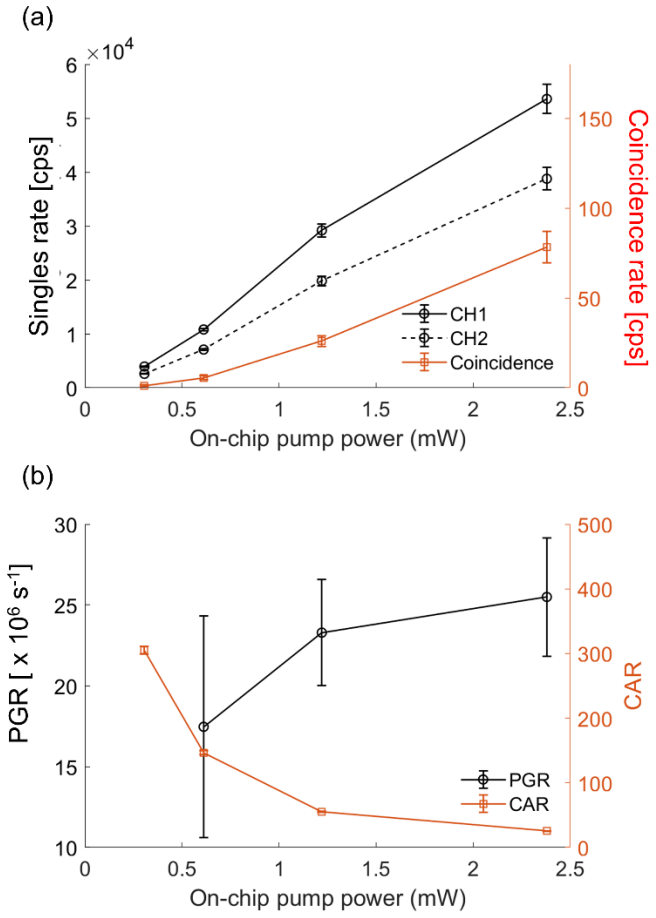

Fig. 4 (a) Singles rates and coincidences rates in units of counts per second (cps). Error bars are one half standard deviation of the measurement. (b) Pair generation rates (off-chip) and CAR of the photon source. Error bars are one half standard deviation of the measurement. The compound standard deviation of pair generation rates is propagated from singles rates and coincidence rates, which are used to calculate PGR by PGR = S1× S2 /C. The CAR at the lowest and highest power levels are 305 and 25 respectively.

Fig. 4(a) shows the measured off-chip singles rates and coincidence rates as a function of the pump power coupled onto the chip (i.e., at the start of the feeder waveguide), with differences in the values a consequence of the different losses through the filters versus wavelength (3.6 dB and 7.2 dB at the signal and idler wavelengths). An estimate of the on-chip

pair generation rate (PGR) was calculated by PGR = S1×S2/C, where S1 and S2 are signal and idler single rates (units: Hz) and C is the coincidence rate (units: Hz). The dependence of PGR on the input pump power is not quadratic, since the input pump power is relatively high and two-photon absorption cannot be ignored. The advantage of this method of calculating PGR is that it normalizes out the temporal fluctuations in the fiber-to-waveguide coupling coefficients over long measurement periods. Low values of the denominator (measured coincidence rate) are dropped; therefore, the PGR is not indicted in Fig. 4(b) for the lowest pump power, 0.25 mW. This expression over-estimates the true PGR; the difference is given approximately by the rate of the noise photons which are generated linearly with the pump power [10], but these rates are expected to be small, given the insertion loss of the first filter stage near the input edge of the chip, the narrow bandwidth of the resonator and the inclusion of the pump power reduction filter stage immediately following the microring. In any case, since the rate of the noise photons cannot exceed the measured singles rate [shown in Fig. 4(a)], divided by the coupling losses, the terms ignored in calculating PGR are no more than 1 x 10^6 cps. This is smaller than the errorbars that are already indicated in Fig. 4(b) from the propagation of uncertainties calculation.

In Fig. 4(b), the pair generation rate at the ring and measured CAR is shown as a function of the on-chip pump power. From this data, the in-cavity (internal) spectral brightness of the ring at the highest pump level was calculated to be 6.5×10^{10} cps/mW^2/nm or 5.2×10^8 cps/mW^2/GHz. The spectral brightness of this microring device is three orders of magnitude higher than reported in a ring-with-filter context ($5x10^5$ cps/mW^2/GHz) in Ref. [29]. In fact, the brightness achieved here is similar to that achieved using the brightest stand-alone silicon microdisk resonators [30] and the brightest stand-alone microring resonators reported so far [13], where a different method was used to calculate the PGR. However, higher-than-expected filter losses significantly reduced the number of photon pairs that are coupled to fiber at the chip output; the measured coincidence rates are shown along the right-hand side vertical axis in Fig. 4(a) and are about two orders of magnitude lower than earlier reported using the best stand-alone microrings with a similar Q factor.

Measurements of CAR versus CW on-chip pump power are shown in Fig. 4(b). The cross-correlation function of the arrival times of the two photons in a pair was measured for typical acquisition times of 200 to 1,000 seconds (longer acquisition times for lower singles rates). The counts were binned into histograms, one for each input pump power level. Each histogram peak was fitted by a Gaussian function, whose FWHM was about 25 ps, and the one standard deviation values of the fitting generated the error bars shown in the plots.

The highest CAR was 305 ± 6 measured using an integration time of 1,000 seconds. At the highest power values used here, CAR = 25 ± 0.46 with an integration time of 200 seconds, at a pair generation spectral brightness of 6.5×10^{10} cps/mW^2/nm or, equivalently, 5.2×10^8 cps/mW^2/GHz using a different set of units also widely used. As expected, CAR decreased at higher pump powers, and when the pair generation rate was higher, a shorter integration time was adequate in order to achieve smaller error bars.

Additional Diagnostics

In this batch of fabricated microchips, the losses of the filters as shown in Fig. 5(a) are higher than expected, and were estimated, from separate singulated-chip measurements to be greater than 10 dB for the ASE filter and pump rejector stages, and greater than 3 dB for the photon pair/pump demux stage.

In Fig. 5(b), we compared the same device (the residual pump suppression filter) on a die selected from a passive wafer (no dopants, no metals), and from a die selected from the active wafer. We observe greater degradation of extinction and higher overall transmission loss especially at longer wavelengths, and broadened passbands. This is most likely the result of increased optical loss from the optical waveguide mode interacting with the metal heaters which

were positioned directly above the waveguides in our current design. Indeed, such optical loss would increase at the longer wavelengths, since the optical modes are slightly less confined, and this appears to be the case in the data shown in Fig. 5(b). We believe that the higher-than-expected loss and wider passbands of these filters may have been caused by an error in the deposited oxide thickness between the silicon and metal layers. A future version of the chip can move the metal heaters and feeder electrical lines further away from the optical structures. The thermally-tunable CROW filter architecture is both compact and versatile and can be adapted for applications in both classical and quantum photonics [31-34]. Other types of filters, e.g., Mach-Zehnder interferometers could also be used for optical filtering; such filters may be easier to realize and tune, but typically have a narrower passband and take more space in the chip, which may lead to crosstalk among different stages. Despite the present limitations, the opto-electronic integrated chip which we measured from this batch of fabricated wafers was already able to obtain correlated photon pairs, and we believe future filtering improvements can be achieved by using existing silicon photonics fabrication technology.

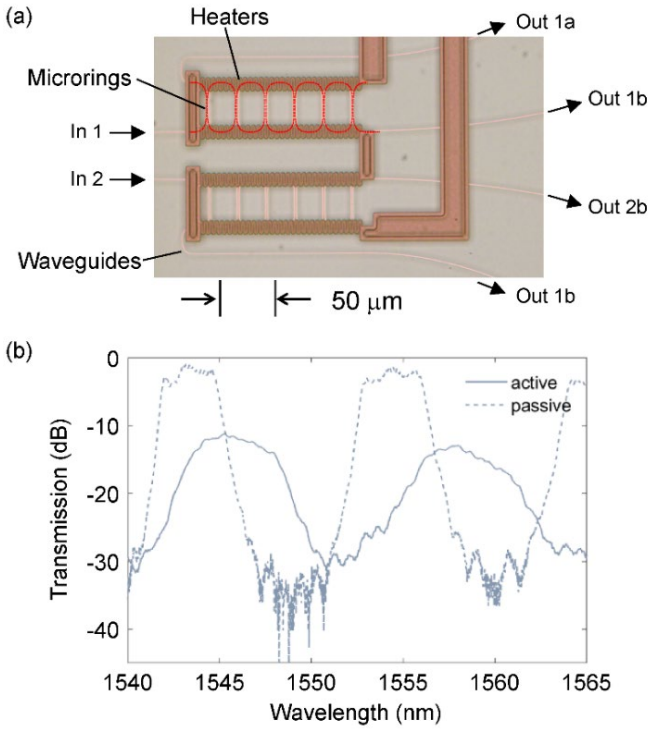

Fig. 5 (a) Microscope image of two channels of fifth-order microring filters with metal heaters for thermal tuning. The outline of some of the racetrack resonators is indicated by a red dashed outline. (b) The drop port transmission measured from a separated segment of the chip. A comparison between the same device fabricated on a passive and active wafer is presented here, which shows the degraded extinction, increased bandwidth and higher loss in the latter case.

4. Conclusion

In summary, we have reported progress towards the goal of a fully-integrated microchip-scale quantum light source that could be used to generate high brightness photon pairs at telecommunication wavelengths. Once fully realized, such microchips which integrate the pair generation stage with various optical filters which perform several different functions, may be useful for widespread practical usage, and in-network deployment of quantum silicon photonic devices.

Funding

NSF (CNS-1525090, EFMA-1640968); IBM PhD Fellowship Program; NASA (Grant Nos. NNX16AD14G and 80NSSC17K0166).

Disclosures

The authors declare no conflicts of interest.

References

1. P. Kok, W. J. Munro, K. Nemoto, T. C. Ralph, J. P. Dowling and G. J. Milburn, "Linear optical quantum computing with photonic qubits," Rev. Mod. Phys. **79**, 135-174 (2007).
2. X. Qiang, X. Zhou, J. Wang, C. M. Wilkes, T. Loke, S. O'Gara, L. Kling, G. D. Marshall, R. Santagati, T. C. Ralph and J. B. Wang, "Large-scale silicon quantum photonics implementing arbitrary two-qubit processing," Nat. Photonics **12**, 534 (2018).
3. A. W. Elshaari, I. E. Zadeh, A. Fognini, M. E. Reimer, D. Dalacu, P. J. Poole, V. Zwiller and K. D. Jöns, "On-chip single photon filtering and multiplexing in hybrid quantum photonic circuits" Nat. Commun. **8**, 379 (2017).
4. S. Paesani, Y. Ding, R. Santagati, L. Chakhmakhchyan, C. Vigliar, K. Rottwitt, L. K. Oxenløwe, J. Wang, M. G. Thompson and A. Laing, "Generation and sampling of quantum states of light in a silicon chip" Nat. Physics **15**, 925–929 (2019).
5. N. C. Harris, G. R. Steinbrecher, M. Prabhu, Y. Lahini, J. Mower, D. Bunandar, C. Chen, F. N. C. Wong, T. Baehr-Jones, M. Hochberg, S. Lloyd and D. Englund "Quantum transport simulations in a programmable nanophotonic processor" Nat. Photonics **11**, 447–452 (2017).
6. Y. Chen, J. Zhang, M. Zopf, K. Jung, Y. Zhang, R. Keil, F. Ding and O. G. Schmidt, "Wavelength-tunable entangled photons from silicon-integrated III-V quantum dots," Nat. Commun. **7**, 10387 (2016).
7. I. Aharonovich, C. Zhou, A. Stacey, J. Orwa, S. Castelletto, D. Simpson, A. D. Greentree, F. Treussart, J.-F. Roch and S. Prawer, "Enhanced single-photon emission in the near infrared from a diamond color center," Phys. Rev. B **79**, 235316 (2009).
8. J. E. Sharping, K. F. Lee, M. A. Foster, A. C. Turner, B. S. Schmidt, M. Lipson, A. L. Gaeta, and P. Kumar, "Generation of correlated photons in nanoscale silicon waveguides," Opt. Express **14**, 12388–12393 (2006).
9. J. Chen, Z. H. Levine, J. Fan, and A. L. Migdall, "Frequency-bin entangled comb of photon pairs from a silicon-on-insulator micro-resonator," Opt. Express 19, 1470–1483 (2011).
10. E. Engin, D. Bonneau, C. M. Natarajan, A. S. Clark, M. G. Tanner, R. H. Hadfield, S. N. Dorenbos, V. Zwiller, K. Ohira, N. Suzuki, H. Yoshida, N. Iizuka, M. Ezaki, J. L. O'Brien, and M. G. Thompson, "Photon pair generation in a silicon micro-ring resonator with reverse bias enhancement," Opt. Express **21**, 27826–27834 (2013).
11. R. Wakabayashi, M. Fujiwara, K.-i. Yoshino, Y. Nambu, M. Sasaki, and T. Aoki, "Time-bin entangled photon pair generation from Si micro-ring resonator," Opt. Express **23**, 1103–1113 (2015).
12. S. F. Preble, M. L. Fanto, J. A. Steidle, C. C. Tison, G. A. Howland, Z. Wang, and P. M. Alsing, "On-chip quantum interference from a single silicon ring-resonator source," Phys. Rev. Appl. **4**, 021001 (2015).
13. C. Ma, X. Wang, V. Anant, A. D. Beyer, M. D. Shaw and S. Mookherjea, "Silicon photonic entangled photon-pair and heralded single photon generation with CAR > 12,000 and g˝(2)(0) < 0006," Opt. Express **25**, 32995 (2017).
14. X. Wang, C. Ma, R. Kumar, P. Doussiere, R. Jones, H. Rong and S. Mookherjea "Photon Pair Generation Using a Silicon Hybrid Laser" APL Photonics **3**, 106104 (2018).
15. M. J. Collins, C. Xiong, I. H. Rey, T. D. Vo, J. He, S. Shahnia, C. Reardon, T. F. Krauss, M. J. Steel, A. S. Clark and B. J. Eggleton "Integrated spatial multiplexing of heralded single-photon sources" Nat. Commun. **4**, 2582 (2013).
16. N. Matsuda, P. Karkus, H. Nishi, T. Tsuchizawa, W. J. Munro, H. Takesue and K. Yamada, "On-chip generation and demultiplexing of quantum correlated photons using a silicon-silica monolithic photonic integration platform" Opt. Express **22**, 22831-22840 (2014).
17. J.-M. Lee, W.-J. Lee, M.-S. Kim, and J. J. Ju, "Noise Filtering for Highly Correlated Photon Pairs From Silicon Waveguides," J. Lightwave Technol. 37, 5428-5434 (2019).
18. A. S. Rab, E. Polino, M. Valeri, P. Mataloni, N. Spagnolo, F. Sciarrino, S. Atzeni, G. Corrielli, A. Crespi and R. Osellame, "Integrated source of entangled photon pair at telecom wavelength" in *Proc. Quantum Information and Measurement* T5A-8 (2019).
19. J. Chen, Z. H. Levine, J. Fan, and A. L. Migdall "Frequency-bin entangled comb of photon pairs from a silicon-on-insulator micro-resonator" Opt. Express **19**, 1470-1483 (2011).
20. R. Kumar, J. R. Ong, J. Recchio, K. Srinivasan, and S. Mookherjea, "Spectrally multiplexed and tunable wavelength photon pairs at 1.55 μm from a silicon coupled-resonator optical waveguide," Opt. Lett. **38**, 2969–2971 (2013).
21. M. Savanier, R. Kumar and S. Mookherjea, "Optimizing photon-pair generation electronically using a pin diode incorporated in a silicon microring resonator" Appl. Phys. Lett. **107**, 131101 (2015)

22. Agilent 81480A, and Agilent 81680A, 81640A, 81682A, 81642A and 81689A User's Guide (2001). Available online at https://www.keysight.com/upload/cmc_upload/All/tlsm0101.pdf
23. M. Piekarek, D. Bonneau, S. Miki, T. Yamashita, M. Fujiwara, M. Sasaki, H. Terai, M. G. Tanner, C. M. Natarajan, R. H. Hadfield, J. L. O'Brien and M. G. Thompson, "High-extinction ratio integrated photonic filters for silicon quantum photonics," Opt. Lett. **42**, 815-818 (2017).
24. N. C. Harris, D. Grassani, A. Simbula, M. Pant, M. Galli, T. Baehr-Jones, M. Hochberg, D. Englund, D. Bajoni and C. Galland, "Integrated source of spectrally filtered correlated photons for large-scale quantum photonic systems" Phys. Rev. X **4**, 041047 (2014).
25. C. Ma, X. Wang and S. Mookherjea "Photon-pair and heralded single photon generation initiated by a fraction of a 10 Gbps data stream" Opt. Express **26**, 22904-22915 (2018).
26. A. Tanaka, M. Fujiwara, S. W. Nam, Y. Nambu, S. Takahashi, W. Maeda, K.-i. Yoshino, S. Miki, B. Baek, Z. Wang, A. Tajima, M. Sasaki and A. Tomita, "Ultra fast quantum key distribution over a 97 km installed telecom fiber with wavelength division multiplexing clock synchronization" Opt. Express **16**, 11354-11360 (2008).
27. J. R. Ong, R. Kumar and S. Mookherjea, "Ultra-high-contrast and tunable-bandwidth filter using cascaded high-order silicon microring filters" IEEE Photon. Technol. Lett. **25**, 1543-1546 (2013).
28. S. Mookherjea and H. R. Grant "High dynamic range microscope infrared imaging of silicon nanophotonic devices." Opt. Lett. **37**, 4705-4707 (2012)
29. D. Oser, S. Tanzilli, F. Mazeas, C. Alonso-Ramos, X. Le Roux, G. Sauder, X. Hua, O. Alibart, L. Vivien, É. Cassan, L. Labonté, "High-quality photonic entanglement out of a stand-alone silicon chip", npj Quantum Information **6**, 31 (2020).
30. W. C. Jiang, X. Lu, J. Zhang, O. J. Painter and Q. Lin "Silicon-chip source of bright photon pairs" Opt. Express **23**, 20884-20904 (2015).
31. J. R. Ong, R. Kumar and S. Mookherjea "Silicon micro-ring based wavelength converter with integrated pump and signal suppression" Opt. Lett. **39**, 4439-4441 (2014).
32. R. R. Kumar, X. Wu, and H. K. Tsang, "Compact high-extinction tunable CROW filters for integrated quantum photonic circuits," Opt. Lett. **45**, 1289-1292 (2020).
33. K. Xu, J.-Y. Sung, C. Y. Wong, Z. Cheng, C. W. Chow and H. K. Tsang, "Optical Nyquist filters based on silicon coupled resonator optical waveguides", Optics Commun. **329**, 23 (2014).
34. H. Jayatilleka, K. Murray, M.Á. Guillén-Torres, M. Caverley, R. Hu, N. A. F. Jaeger, L. Chrostowski, and S. Shekhar, "Wavelength tuning and stabilization of microring-based filters using silicon in-resonator photoconductive heaters," Opt. Express 23, 25084-25097 (2015)